THE JOURNAL OF PHYSICAL CHEMISTRY A
A JOURNAL OF THE AMERICAN CHEMICAL SOCIETY

pubs.acs.org/JPCA

Article

Quantum Chemical Investigation of the Cold Water Dimer Spectrum in the First OH-Stretching Overtone Region Provides a New Interpretation

Emil Vogt, Irén Simkó, Attila G. Császár, and Henrik G. Kjaergaard*

Cite This: *J. Phys. Chem. A* 2023, 127, 9409−9418

Read Online

ACCESS | Metrics & More | Article Recommendations | Supporting Information

ABSTRACT: Intramolecular vibrational transition wavenumbers and intensities were calculated in the fundamental HOH-bending, fundamental OH-stretching, first OH-stretching-HOH-bending combination, and first OH-stretching overtone ($\Delta v_{OH} = 2$) regions of the water dimer's spectrum. Furthermore, the rotational−vibrational spectrum was calculated in the $\Delta v_{OH} = 2$ region at 10 K, corresponding to the temperature of the existing jet-expansion experiments. The calculated spectrum was obtained by combining results from a full-dimensional (12D) vibrational and a reduced-dimensional vibrational−rotational-tunneling model. The $\Delta v_{OH} = 2$ spectral region is rich in features due to contributions from multiple vibrational−rotational-tunneling sub-bands. Origins of the experimental vibrational bands depend on the assignment of the observed sub-bands. Based on our calculations, we assign the observed sub-bands, and our reassignment leads to new values for the vibrational band origins of the free donor and antisymmetric acceptor OH-stretching first overtones of ∼7227 and ∼7238 cm^{-1}, respectively. The observed bands with origins at 7192.34 and ∼7366 cm^{-1} are assigned to the symmetric acceptor OH-stretching first overtone and the OH-stretching combination of the donor, respectively.

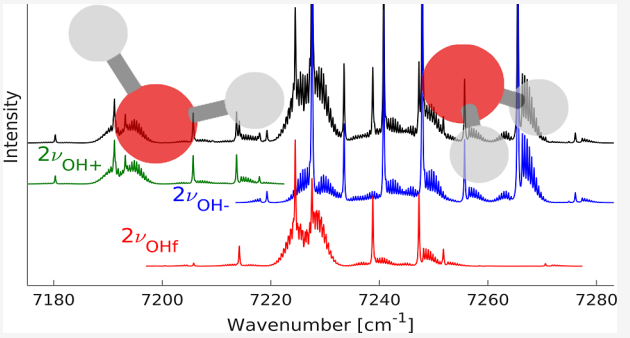

INTRODUCTION

The spectroscopy of water dimer, $(H_2O)_2$, has been of interest for decades, as reviewed in refs 1−4. Since the first infrared observation of water dimer transitions in an N_2 matrix-isolation study, multiple jet-expansion gas-phase, matrix isolation, and He-droplet spectra containing water dimer have been published.[5−15] The cold environment in these experiments favors complex formation. However, spectral interference from larger complexes or complexes formed with the jet-expansion carrier gas is common and complicates the spectral assignment.[16,17]

A number of jet-expansion spectra of the OH-stretching and HOH-bending regions of water dimer were published between 1980 and 2000.[6−8,18,19] A high-resolution spectrum from 1989 highlighted the rotational-tunneling structure in the OH-stretching fundamental region.[7] More recently, the spectral range probed has been extended to the first OH-stretching overtone ($\Delta v_{OH} = 2$) region in two seminal jet-expansion experiments.[10,14] The first spectrum was recorded in the 7100−7300 cm^{-1} range with an Ar carrier gas using the infrared-ultraviolet vibrationally mediated dissociation technique.[10] Based on simulations of the observed rotational−vibrational profiles, a rotational temperature of 7 ± 3 K was determined.[10] In the second jet-expansion study,[14] a set of continuous-wave cavity ring-down (CRD) spectra were recorded, using either krypton, argon, or neon as the carrier gas. The use of different noble gases allowed for a clear distinction of transitions originating from water dimer and those from bimolecular complexes between H_2O and the carrier-gas atoms. Two narrow wavenumber ranges were covered: 7188−7285 and 7357−7386 cm^{-1}. Based on simulations of the observed rotational−vibrational profiles, a rotational temperature of 10 ± 3 K was determined.[14] The assignment of the observed bands in these two cold experiments was, in part, guided by transition wavenumbers and intensities from matrix-isolation experiments and earlier calculations.[12,20−23] These vibrational calculations were based on reduced-dimensional local mode models of the intramolecular modes and either ignored the intermolecular modes or included part of their effect in an approximate way.[20−23]

An unambiguous assignment of the observed water dimer transitions is challenging without aid from quantum-chemical calculations. Upon complex formation, six low-frequency intermolecular vibrational modes arise. The intermolecular modes describe the relative orientation and distance between

Received: June 1, 2023
Revised: September 28, 2023
Published: November 6, 2023

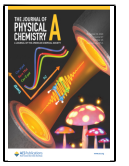

the two H_2O units and are coupled to the high-frequency OH-stretching and HOH-bending (intramolecular) modes. The challenge of calculating accurate water dimer spectra arises in part due to the low-energy tunneling barriers that connect the eight equivalent versions on the potential energy surface (PES).[24,25] A range of 12D PESs are applicable to water dimer and have been used both for spectroscopic purposes and to describe the pairwise interaction of water molecules in larger water clusters.[26−33] The PES of water dimer is highly anharmonic, and the vibrational−rotational-tunneling (VRT) states are difficult to describe even with advanced models. The dissociation energy of water dimer is low, $\tilde{D}_0 \approx 1100$ cm^{-1} ($\tilde{D}_e \approx 1760$ cm^{-1}), and even the first intramolecular transitions are above the dissociation energy.[27,29,34−36] Accurate variational (-type) nuclear-dynamics computations have been carried out for several PESs.[29,30,37−41] These calculations have revealed the energy-level structure of the VRT states, which has been paramount to advance the understanding of the spectra of water dimer and other weakly bound complexes.

In this study, we utilize a recently developed effective Hamiltonian-based model termed VibMEMIC (Vibrational Many-mode Expansion Model in Internal Coordinates),[42] but here, use the term *n*-mode instead of many-mode. The VibMEMIC model is a finite-basis-representation model that uses 3-mode representations of the kinetic energy operator and the PES expressed in curvilinear internal coordinates. Until now, VibMEMIC has been employed to compute the fundamental transition wavenumbers of the intramolecular modes of water dimer in 12D.[42] As a further development, the full-dimensional (12D) vibrational VibMEMIC calculations are here extended to include transition intensities using 3-mode representations of the Cartesian components of the dipole-moment function (DMF). Rotations and tunneling splittings are taken into account with reduced-dimensional models, employing the GENIUSH code.[43−45] The results from the two models are combined to yield a spectrum of water dimer in the $\Delta\nu_{OH} = 2$ region at $T = 10$ K. Based on our calculated spectrum, we assign the VRT sub-bands observed in the existing jet-expansion experiments.[10,14]

THEORETICAL SECTION

VibMEMIC Vibrational Model. The VibMEMIC calculations utilized the CCSD(T)-F12a/cc-pVTZ-F12 PES and DMF published in the repository of ref 42, which are evaluated at evenly spaced grids. We have previously shown that accurate OH-stretching fundamental and overtone transition wavenumbers and intensities can be calculated with CCSD(T)-F12 level PESs and DMFs as compared with experiments.[4,46−49]

A detailed description of the VibMEMIC model can be found in ref 42. Here, we provide only a summary of the approximations characterizing the model and a brief description of the extension of the code used to calculate the vibrational transition intensities. The VibMEMIC model uses a finite-basis representation of the Podolsky Hamiltonian with 3-mode representations of the PES and the *G*-matrix elements of the kinetic-energy operator. The 3-mode representations allow us to couple all 12 vibrational modes of water dimer due to the reduced computational work associated with this approximate form of the PES and *G*-matrix elements. Previously, *n*-mode representations have been used in conjunction with rectilinear coordinates, which alleviates the need to expand the *G*-matrix elements. We refer the reader to refs 50 and 51 for a detailed description of the *n*-mode representation.

All matrix elements are calculated with mode-specific quadrature grids with 101 points per mode. The 12 curvilinear internal coordinates are the same as in ref 42 and are defined in Figure S1 of this paper. The reference structure for the *n*-mode expansions is the CCSD(T)-F12a/cc-pVTZ-F12 optimized structure, but with the OH bond lengths of the donor defined as the average of the two donor OH bond lengths.

The combination of the chosen reference structure and the coordinate definition facilitates the use of the G_8 molecular symmetry (MS) group,[25] which includes exchange of the hydrogens within the monomers and spatial inversion but not the exchange of the two monomers. The 12D basis functions are symmetry-adapted linear combinations of products of 1D eigenfunctions. The 1D eigenfunctions are obtained by solving the 1D Schrödinger equation for each mode, with the potential energy and *G*-matrix element curves calculated from the reference structure. We use the 1D eigenfunctions of the free OH stretch (OH_f) for both OH_f and the bound OH stretch (OH_b) to preserve the symmetry properties of the OH-stretches of the donor. The 12D basis functions transform according to the irreducible representations of the G_8 MS group (A_1', A_1'', A_2', A_2'', B_1', B_1'', B_2', and B_2''), and the Hamiltonian matrix takes a block-diagonal form with a total of eight blocks. Energy ceilings and polyad truncations are used to control the size of the basis and are defined such that the different blocks of the Hamiltonian are of a similar size.

To converge the OH-stretching states in the first OH-stretching overtone region, additional approximations were made to limit the number of coupling terms between the intramolecular and intermolecular modes (Section S2). The approximations concern the exclusion of specific PES and *G*-matrix coupling terms that were previously found to have a limited impact on the intramolecular transition wavenumbers, which we are focusing on. The calculated OH-stretching transition wavenumbers are converged to better than 0.5 cm^{-1}, using $\sim 2.6 \times 10^5$ 12D basis functions.

To calculate the transition intensities, the dipole moment matrix for each Cartesian component needs to be calculated. The operators for the dipole moment matrix elements are the Cartesian components of the DMF. Similar to the potential energy and *G*-matrix surfaces, the three components of the DMF are also approximated with 3-mode representations in curvilinear internal coordinates. Cubic splines were used to obtain the components of the CCSD(T)-F12a/cc-pVTZ-F12 DMF at the same quadrature points as those used for the evaluation of the kinetic and potential energy matrix elements. To utilize symmetry, the DMF is expressed along the *A*, *B*, and *C* principal axes. The *A*- and *C*-components of the DMF transform as the irreducible representation A_1', whereas the *B*-component transforms as A_2'. The *A*- and *C*-components of the dipole-moment matrix are block-diagonalized into eight blocks. The dipole-moment matrix for the *B*-component consists of four 2×2 blocks, with nonzero off-diagonal sub-blocks. The symmetry-adapted dipole-moment matrix for each Cartesian component is constructed from linear combinations of smaller matrices. Construction of the linear combinations of matrices is demanding in computational time, but significantly reduces the memory requirements relative to doing an orthogonal transformation of the full dipole-moment matrix.

Due to the 3-mode representation of the PES and the *G*-matrix elements, the VibMEMIC model is suitable to and developed for the accurate computation of the intramolecular transitions from the ground state to the lowest state of the

https://doi.org/10.1021/acs.jpca.3c03705
J. Phys. Chem. A 2023, 127, 9409−9418

tunneling multiplet. The approximate nature of the 3-mode representation of the PES and the G-matrix elements leads to a breakdown of the exact permutation-inversion symmetry but has a limited effect on the calculated intramolecular band origins.[42] Changes in the tunneling splitting with excitations of the intramolecular modes can therefore not be described with the VibMEMIC model, and the contributions to the spectrum simulated from the four blocks of the DMF are practically identical. Here, we present the transition wavenumbers and intensities calculated for a single (2×2) block. To simulate the rotation-tunneling sub-bands of the individual OH-stretching transitions of $\Delta v_{OH} = 2$, we use a set of reduced-dimensional rotational−vibrational simulations performed with the GENIUSH code.

Rotation-Tunneling Model. Rotations and tunneling splittings for the ground and the excited vibrational states have been taken into account through the use of reduced-dimensional models and the GENIUSH code.[43−45] Tunneling causes each "traditional" rotational−vibrational energy level of water dimer to split into eight VRT levels.[24,25] The largest splittings correspond to "acceptor tunneling" (interchange of the hydrogens of the acceptor), and the values depend strongly on the K_a asymmetric-top quantum number. This splitting divides the eight VRT states into two bundles of four states, which, for $K_a = 0$, are separated by ∼11 cm^{-1} in the vibrational ground state. Our model of rotation and tunneling includes the J- and K_a-dependence of the energy and acceptor-tunneling for the ground and excited vibrational states. The other two tunneling pathways, the "donor tunneling" and the "donor−acceptor interchange", cause significantly smaller splittings (∼1 cm^{-1}) and are not accounted for in our model.[2]

The symmetry-adapted version[45] of the quasi-variational nuclear-motion code GENIUSH[43,44] employed allows the computation of tunneling splittings as well as the determination of $J > 0$ rotational−vibrational energy levels. These computations utilized the MB-pol PES.[29] Computations were performed by using a 5D reduced-dimensional model chosen to describe the acceptor tunneling. The active coordinates were the three intermolecular Euler angles (θ, ϕ, and α in Figure S1) and the two OH bond lengths of either the donor or the acceptor, depending on which one is excited. The inactive coordinates were fixed to their equilibrium values (Section S3). It was necessary to use a reduced-dimensional model to make the $J > 0$ computations feasible in the OH-stretching overtone region. The 5D model chosen includes only the acceptor tunneling; therefore, each rotational−vibrational state is split into two states, which is equivalent to treating the four states in the two bundles in the full-dimensional picture as if they were degenerate.

Rotational−vibrational computations were performed for $J \leq 3$ for the vibrational ground state and for $J = 0$ and 1 in the OH-stretching overtone region. The $J = 2$ and 3 energies in the OH-stretching overtone region were estimated based on the computed energies (Section S3). The absolute energies obtained within this model have large errors due to the neglect of the coupling of the intramolecular stretches with the intramolecular bends and the three inactive intermolecular modes. However, the tunneling splittings and the rotational energy contributions are expected to be much more accurate, partly due to error cancellation. The final VRT energy levels are obtained by shifting all of the GENIUSH energies (MB-pol PES) corresponding to a given vibration by the same amount. The shift is chosen such that, for $J = 0$, the lower energy of the acceptor tunneling doublet is equal to the vibrational energy computed with VibMeMIC in the 12D model [CCSD(T)-F12a/cc-pVTZ-F12 PES]. The uncertainty of the rotation-tunneling energy-level pattern is expected to be ∼1 cm^{-1}.

Computation of the Spectrum. We constructed the simulated spectrum in two steps. First, we calculated the total intensity corresponding to each (GS, K_a, p) → (v, K_a', p) sub-band, where p denotes component (1) or (2) of the acceptor tunneling doublet. The Q branch ($\Delta J = 0$ transition) of the sub-band is centered at $E_p(v, J', K_a') - E_p(\mathrm{GS}, J, K_a)$ with $J = J' = \max(K_a, K_a')$. In the second step, we introduced a small wavenumber shift (+6 cm^{-1}) in the transitions and convoluted them with a suitable rotational profile to improve comparison with the measured spectrum.

The intensity of a rovibrational transition between the i = (GS, J, K_a, p) and f = (v, J', K_a', p) states is calculated as

$$I(i \to f) = c_0 \frac{\tilde{\nu}}{Q(T)} \exp\left(-\frac{E_i}{k_B T}\right)\left(1 - \exp\left(-\frac{E_f - E_i}{k_B T}\right)\right) S(i \to f) \quad (1)$$

where $c_0 = (8\pi^2)/(4\pi\varepsilon_0 3hc)$ is a constant factor, $\tilde{\nu} = (E_f - E_i)/(hc)$ is the transition wavenumber, $Q(T)$ is the partition function, and $S(i \to f)$ is the line strength. Water dimer is nearly a prolate symmetric top. If we apply this approximation, the rotations and the vibrations are separated, and the line strength is calculated as

$$S(i \to f) = g_p(2J' + 1)(2J + 1) \left| \sum_{\sigma} \mu_m^{(1,\sigma)} (-1)^K \begin{pmatrix} J & 1 & J' \\ K_a & \sigma & -K_a' \end{pmatrix} \right|^2 \quad (2)$$

where (:::) is the Wigner-3J symbol, g_p is the nuclear spin statistical weight, and $\mu_m^{(1,\sigma)}$ are the body-fixed components of the transition dipole moment expressed in spherical basis, with $\mu_m^{(1,0)} = \mu_A$ and $\mu_m^{(1,\pm 1)} = (\mp \mu_C - i\mu_B)/\sqrt{2}$, where μ_A, μ_B, and μ_C are the components in the principal axis system. At the temperature of the experiments (∼10 K), only $K_a = 0$, 1, and 2 states have significant population, and the partition function is

$$Q(T) = \sum_{p=1}^{2} \sum_{K_a=-2}^{2} \sum_{J=|K_a|}^{\infty} g_p(2J + 1) e^{-E_p(\mathrm{GS}, J, K_a)} \quad (3)$$

In order to obtain the total intensity of a given (GS, K_a, p) → (v, K_a', p) band, we have to sum for J and J'. We introduce the following approximations: we neglect the $(1 - \exp(-(E_f - E_i)/(k_B T)))$ term as it is close to 1 for the OH-stretching overtone transitions and use the vibrational transition wavenumber ($\tilde{\nu}^{vib}$), computed with VibMEMIC, for all transitions within a given vibrational transition. Then, the intensity formula can be written as

https://doi.org/10.1021/acs.jpca.3c03705
J. Phys. Chem. A 2023, 127, 9409−9418

$$I^{\mathrm{tot}}((\mathrm{GS}, K_a, p) \rightarrow (v, K_a', p)) = \sum_{J=|K_a|}^{\infty} \sum_{J'=J-1}^{J+1}$$

$$I((\mathrm{GS}, J, K_a, p) \rightarrow (v, J', K_a', p)) \approx c_0 \frac{\tilde{\nu}^{\mathrm{vib}}}{Q(T)} |\mu_m^{(1,\sigma)}|^2$$

$$\sum_{J=|K_a|}^{\infty} g_p(2J+1) \left(\sum_{J'=J-1}^{J+1} (2J'+1) \begin{pmatrix} J & 1 & J' \\ K_a & \sigma & -K_a' \end{pmatrix}^2 \right)$$

$$e^{-E_p(\mathrm{GS},J,K_a)/(k_B T)} \quad (4)$$

where $\sigma = -K_a + K_a'$. The different J levels stacked on a given K_a level follow a rigid-rotor energy pattern, i.e.,

$$E_p(\mathrm{GS}, J, K_a) = E_p(\mathrm{GS}, |K_a|, K_a) + B(J(J+1) - |K_a|(|K_a|+1)) \quad (5)$$

Equation 4 can be simplified, since

$$\sum_{J'=J-1}^{J+1} (2J'+1) \begin{pmatrix} J & 1 & J' \\ K_a & (-K_a + K_a') & -K_a' \end{pmatrix}^2 = 1 \quad (6)$$

and therefore

$$\frac{1}{Q(T)} \sum_{J=|K_a|}^{\infty} g_p(2J+1) e^{-E_p(\mathrm{GS},J,K_a)/(k_B T)} \approx \frac{1}{Q^{VT}(T)} g_p e^{-E_p(\mathrm{GS},|K_a|,K_a)/(k_B T)} \quad (7)$$

where

$$Q^{\mathrm{VT}}(T) = \sum_{p=1}^{2} \sum_{K_a=-2}^{2} g_p e^{-E_p(\mathrm{GS},|K_a|,K_a)} \quad (8)$$

is the vibrational-tunneling partition function calculated after neglecting the different J energy levels. Finally, we obtain

$$I^{\mathrm{tot}}((\mathrm{GS}, K_a, p) \rightarrow (v, K_a', p)) \approx c_0 \frac{\tilde{\nu}^{\mathrm{vib}}}{Q^{\mathrm{VT}}(T)} |\mu_m^{(1,\sigma)}|^2 g_p e^{-E_p(\mathrm{GS},|K_a|,K_a)/(k_B T)} \quad (9)$$

For $\Delta K_a = 0$ transitions, the expression becomes

$$I^{\mathrm{tot}}((\mathrm{GS}, K_a, p) \rightarrow (v, K_a, p)) \approx c_0 \frac{\tilde{\nu}^{\mathrm{vib}}}{Q^{\mathrm{VT}}(T)} |\mu_A|^2 g_p e^{-E_p(\mathrm{GS},|K_a|,K_a)/(k_B T)} \quad (10)$$

and for $\Delta K_a = \pm 1$ transitions

$$I^{\mathrm{tot}}((\mathrm{GS}, K_a, p) \rightarrow (v, K_a \pm 1, p)) \approx c_0 \frac{\tilde{\nu}^{\mathrm{vib}}}{Q^{\mathrm{VT}}(T)} \frac{(|\mu_C|^2 + |\mu_B|^2)}{2} g_p e^{-E_p(\mathrm{GS},|K_a|,K_a)/(k_B T)} \quad (11)$$

Table S10 contains the computed VRT transitions and their relative intensities for the most intense vibrational bands in the $\Delta\nu_{OH} = 2$ region. Once we obtained the total intensity of the $(\mathrm{GS}, K_a, p) \rightarrow (v, K_a', p)$ sub-bands and determined the wavenumber shifts and transition dipole moments, we convoluted the $K_a \rightarrow K_a'$ transitions with rigid-rotor rotational profiles of the sub-bands based on K_a and K_a'. The A-, B-, and C-type rigid-rotor profiles of the $K_a \rightarrow K_a'$ transitions were calculated with PGOPHER with the rotational constants of the CCSD(T)-F12a/cc-pVTZ-F12 reference structure.[42,52] Each VRT transition was subsequently convoluted with a Lorentzian line-profile with a full width at half-maximum of 0.2 cm^{-1}.

RESULTS AND DISCUSSION

In Tables 1 and 2, the 6D and 12D VibMEMIC calculated transition wavenumbers and absolute transition intensities are shown for the OH-stretching transitions in the $\Delta\nu_{OH} = 1$ and $\Delta\nu_{OH} = 2$ regions, respectively. We use a local mode notation, and the symmetric and antisymmetric acceptor OH-stretching modes are abbreviated as OH_+ and OH_-, respectively. The transition intensities are expressed as dimensionless oscillator strengths, f. The 12D results for the HOH-bending and the first OH-stretching-HOH-bending combination regions are shown in Tables S1 and S2, respectively. A comprehensive list of computed transitions in the different intramolecular regions is provided in Table S4. The 6D model includes all intramolecular modes but none of the intermolecular modes (the intermolecular coordinates are fixed to their reference value). The differences between the results obtained with the 6D and 12D models reflect the effect of including the intermolecular modes in the vibrational model. As expected, the largest differences are seen for transitions associated with OH_b.[22,23,53] Upon hydrogen bond formation, the OH_b-stretching transitions redshift relative to the corresponding OH-stretching transitions of the isolated monomer.[54] If the intermolecular modes are not included in the vibrational model, the calculated redshift is overestimated. Inclusion of the intermolecular modes, especially those that partially break the hydrogen bond, results in a lesser redshift of the calculated OH_b-stretching transitions.[22,53] This was originally shown for water dimer with a set of reduced-dimensional vibrational models which employed n-mode representations up to 4-mode of the HBB2 PES in normal coordinates.[53] In ref 53, all six intramolecular modes were included in all calculations, and three of the six intermolecular modes were sequentially added to the model. The redshift of the bound OH-stretching fundamental systematically decreased upon inclusion of the intermolecular modes. These earlier models are similar to our full-dimensional vibrational model, where we utilize 3-mode representations in curvilinear internal coordinates.

In our 6D model, the calculated transition wavenumber of the bound OH-stretching fundamental transition (ν_{OH_b}) is 3555.5 cm^{-1}. In the 12D model, the transition wavenumber of ν_{OH_b} changes to 3599.0 cm^{-1}, which compares well with the observed (jet-cooled) transition wavenumber of 3601 cm^{-1}.[8]

Table 1. Calculated Transition Wavenumbers, $\tilde{\nu}$, and Oscillator Strengths, f, for the OH-Stretching Transitions in the $\Delta\nu_{OH} = 1$ Region Using the CCSD(T)-F12a/cc-pVTZ PES and DMF

	6D model		12D model	
transition	$\tilde{\nu}/\mathrm{cm}^{-1}$	f ($\times 10^{-6}$)	$\tilde{\nu}/\mathrm{cm}^{-1}$	f ($\times 10^{-6}$)
ν_{OH_b}	3555.5	56.2	3599.0	29.0
ν_{OH_+}	3651.6	1.41	3650.6	0.99
ν_{OH_f}	3726.9	14.2	3726.7	15.7
ν_{OH_-}	3746.0	12.4	3742.4	9.65

https://doi.org/10.1021/acs.jpca.3c03705
J. Phys. Chem. A 2023, 127, 9409−9418

Table 2. Calculated Transition Wavenumbers, $\tilde{\nu}$, and Oscillator Strengths, f, for the OH-Stretching Transitions in the $\Delta\nu_{OH} = 2$ Region Using the CCSD(T)-F12a/cc-pVTZ PES and DMF

	6D model		12D model	
transition	$\tilde{\nu}$/cm^{-1}	f ($\times 10^{-8}$)	$\tilde{\nu}$/cm^{-1}	f ($\times 10^{-8}$)
$2\nu_{OH_b}$	6943.4	2.66	7045.9	5.51
$2\nu_{OH_+}$	7185.4	6.78	7187.6	9.28
$2\nu_{OH_f}$	7214.6	31.1	7221.2	24.9
$2\nu_{OH_-}$	7235.9	53.1	7232.1	43.5
$\nu_{OH_b} + \nu_{OH_+}$	7212.1	9.04	7251.3	0.41
$\nu_{OH_b} + \nu_{OH_-}$	7302.3	3.39	7342.3	0.78
$\nu_{OH_b} + \nu_{OH_f}$	7332.9	5.65	7360.9	3.19
$\nu_{OH_f} + \nu_{OH_+}$	7378.9	0.08	7376.8	0.87
$\nu_{OH_+} + \nu_{OH_-}$	7428.1	0.17	7439.5	0.80
$\nu_{OH_f} + \nu_{OH_-}$	7472.9	0.15	7468.9	0.11

We have previously shown that ν_{OH_b} is insensitive to coupling between the intramolecular modes of the donor and acceptor units,[42] and the calculated transition wavenumber of ν_{OH_b} with the 6D model is similar to previous 3D calculations of ν_{OH_b} with other PESs.[22,42,55] In the fundamental OH-stretching region, it is primarily the intensity of ν_{OH_b} that is affected by the inclusion of the intermolecular modes. Earlier second-order vibrational perturbation theory [with CCSD(T)/aug-cc-pVTZ PES and DMF] calculated absolute fundamental intramolecular transition intensities are within 25% of those calculated with our 12D model.[21] With our 12D model, the relative intensities of the four fundamental OH-stretching transitions are in good agreement with relative intensities from various jet-cooled experiments collected in a recent review.[4] This indicates that the 3-mode representation of the DMF is sufficient for computing OH-stretching intensities. Furthermore, the calculated intensities of the fundamental transitions with the 6D model change by <1% when a 2-mode representation of the DMF is used instead of the 3-mode representation. The corresponding change in the first OH-stretching overtone region is <8% for transitions with two quanta of excitation in the same OH-stretching local mode (pure local mode transitions). As expected, the weaker OH-stretching combination transitions are more sensitive to the expansion order of the DMF, and the largest change is seen for the three weakest transitions: 34% for $\nu_{OH_f} + \nu_{OH_+}$, 15% for $\nu_{OH_+} + \nu_{OH_-}$, and 5% for $\nu_{OH_f} + \nu_{OH_-}$. The intensities of the remaining combination transitions change by less than 2%. All OH-stretching transition wavenumbers change by less than 12 cm^{-1} upon using a 2-mode (rather than 3-mode) representation of the PES and G-matrix elements.

In Table 2, the difference between the 6D and 12D models for $2\nu_{OH_b}$ is 103 cm^{-1}, which is approximately twice that for ν_{OH_b}. The difference between the 6D and 12D models for the three OH-stretching combination transitions associated with OH_b is 28−40 cm^{-1}, while it is less than 12 cm^{-1} for the OH-stretching states that are not associated with OH_b. In the 12D model, all OH-stretching combination transitions appear at higher energies relative to those of the pure local mode transitions. In the first OH-stretching overtone region, the relative intensities of the individual transitions change significantly upon inclusion of the intermolecular modes. The shifts of the combination transitions associated with OH_b partially resolve resonances with the pure local mode transitions. The intensities of the combination transitions in the 12D model are smaller than those of the pure local mode transitions. In the spectral region covered by the two jet-expansion experiments, four OH-stretching transitions, $2\nu_{OH_+}$, $2\nu_{OH_f}$, $2\nu_{OH_-}$, and $\nu_{OH_b} + \nu_{OH_f}$, are predicted to be relatively strong. The band origins of $2\nu_{OH_f}$ and $2\nu_{OH_-}$ are predicted to be only ∼11 cm^{-1} apart, which complicates the assignment of the jet-expansion spectra in this region due to the overlapping VRT transitions (Table S10). The VRT transitions of $2\nu_{OH_+}$ and $\nu_{OH_b} + \nu_{OH_f}$ are further away from $2\nu_{OH_f}$ and $2\nu_{OH_-}$ and are expected to have minimal overlap with the VRT transitions of $2\nu_{OH_f}$ and $2\nu_{OH_-}$. Furthermore, $2\nu_{OH_b}$ is also predicted to be relatively strong, but it is located outside of the wavenumber region covered by the experiments.[10,14]

Recently, transition wavenumbers in the OH-stretching fundamental region of water dimer were calculated with a 12D model using the CCpol-8sf PES.[41] The calculated $K_a = 0$ acceptor tunneling splittings of the ground state and three of the four fundamental OH-stretching states are generally larger (3−5 cm^{-1}) than those calculated with our rotation-tunneling model (Table S9). Comparison is not straightforward in the case of the acceptor antisymmetric stretch because the assignment in ref 41 is not unequivocal. The tunneling splittings for $K_a = 1$ are much smaller than for $K_a = 0$, and our calculated ground state tunneling splitting agrees well with earlier calculations.[40] The differences in the calculated $K_a = 0$ tunneling splittings are either due to the approximate nature of our reduced-dimensional calculations or due to differences between the MB-pol PES employed here and the CCpol-8sf PES employed in ref 41. We have recently illustrated relatively large differences for the coupling between intra- and intermolecular vibrations calculated with the MB-pol PES and the CCpol-8sf PESs, but we think that our reduced-dimensional treatment is the primary cause for the discrepancy. However, our reduced-dimensional model is able to capture the magnitude of the acceptor tunneling and its general variation with the vibrational state and K_a, and it turns out to be sufficient for assigning the crowded spectral region of $2\nu_{OH_-}$ and $2\nu_{OH_f}$ (vide infra). As to the band origins, the largest discrepancy between the recent 12D calculations from ref 41 and the transition wavenumbers presented here is ∼10 cm^{-1} for ν_{OH_f}, with the other fundamental OH-stretching transitions being within 3 cm^{-1}. We cautiously attribute the discrepancy for ν_{OH_f} to the employed PESs and refer the reader to our earlier work,[42] in which we calculate and discuss discrepancies in OH-stretching transition wavenumbers obtained with the CCSD(T)-F12a/cc-pVTZ-F12, MB-pol, and CCpol-8sf PESs. The experimental transition wavenumber for ν_{OH_f}, ∼3730 cm^{-1},[7,13,56] is ∼3 cm^{-1} larger than our [VibMEMIC, CCSD(T)-F12/cc-pVTZ-F12 PES] calculated value of 3726.7 cm^{-1}.

In Figure 1, we illustrate the most important rotation-tunneling energy levels for the ground vibrational state and the two close-lying OH-stretching states associated with $2\nu_{OH_f}$ and $2\nu_{OH_-}$. We show only energy levels restricted to $J = K_a$ in

https://doi.org/10.1021/acs.jpca.3c03705
J. Phys. Chem. A 2023, 127, 9409−9418

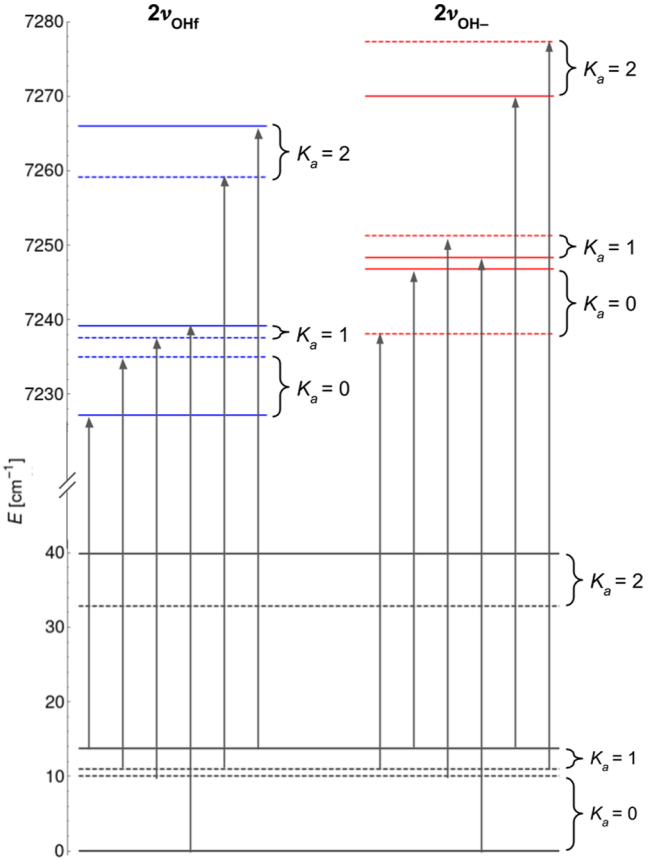

Figure 1. Energy-level diagram of the rotation-tunneling states associated with $2\nu_{OH_f}$ (left, blue) and $2\nu_{OH\_}$ (right, red). The solid and dashed horizontal lines denote components (1) and (2) of the acceptor tunneling splitting, respectively. Perpendicular VRT transitions are shown with arrows in ascending energy order. The ground state energies obtained from the two reduced-dimensional computations are slightly different (Tables S7 and S8); however, this is neglected in the figure.

Figure 1. States with different J values (not shown) are stacked on the $J = K_a$ levels and approximately follow a rigid-rotor energy expression. The two components of the acceptor tunneling doublet are denoted as (1) and (2) and are shown with solid and dashed lines, respectively. For $K_a = 1$ and 2, the order of the two components is swapped as compared to those for $K_a = 0$ and $K_a = 3$ (not shown). If a given vibration is antisymmetric with respect to the mirror plane of the molecule (e.g., $|20\rangle_-$), then the order of the two components is swapped compared to the symmetric vibrations (e.g., the ground state and $|0\rangle_b|2\rangle_f$). The temperature in the two jet-expansion experiments is ~10 K, and transitions originate predominantly from the $K_a = 0$ and 1 levels of the ground vibrational state, with the total intensity of transitions from $K_a = 2$ found to be about 2%. The perpendicular VRT transitions relevant to understanding the experimental spectra are also presented in Figure 1. For $2\nu_{OH_f}$, the parallel VRT transitions also carry intensity, but these are not shown in Figure 1. The calculated transition wavenumbers and intensities of the individual (parallel and perpendicular) VRT transitions are shown in Table S10. Besides the well-known selection rules for parallel and perpendicular rotational−vibrational transitions, it is possible to show that the dipole transitions between components (1) and (2) are forbidden (Section S3). The transitions shown with arrows in Figure 1 are perpendicular transitions with $\Delta J = \pm 1$.

Water dimer is a nearly symmetric top, characterized by equilibrium rotational constants $\tilde{A} \approx 7.2$ cm^{-1} and $\tilde{B} \approx \tilde{C} \approx 0.21$ cm^{-1} [computed at the CCSD(T)-F12a/cc-pVTZ-F12 reference structure], and a Ray asymmetry parameter $\kappa = (2\tilde{B} - \tilde{A} - \tilde{C})/(\tilde{A} - \tilde{C}) \approx -1.0$ (prolate limit). Generic rigid-rotor A-, B-, and C-type bands are shown in Figure 2. The rigid-rotor band profiles help to guide the eye in distinguishing between band types. The rotational band type depends on the direction of the transition dipole moment relative to the rotational axes. The mirror plane in water dimer contains the donor atoms and bisects the HOH-bending angle of the acceptor unit (Figure S1). Vibrational transitions that preserve this mirror plane are A/C-type, whereas transitions related to vibrations that break the mirror plane are B-type. The transition dipole moments calculated with the 12D model are shown in Table S3. For $2\nu_{OH_f}$, the rotational band is A/C-type, whereas for $2\nu_{OH\_}$ it is B-type. Tunneling complicates the simple rigid-rotor picture by giving rise to additional transitions. The simulated spectra of the vibrational bands contain sub-bands corresponding to different $K_a \rightarrow K_a'$ transitions and different acceptor-tunneling components.

In Figure 3, we compare the calculated band profiles of $2\nu_{OH\_}$ and $2\nu_{OH_f}$ with the experimental jet-cooled CRD spectrum between 7220 and 7260 cm^{-1}.[14] In this spectral region, only $2\nu_{OH\_}$ and $2\nu_{OH_f}$ are predicted to have significant intensity (12D results in Table 2). The calculated sub-bands in Figure 3 are labeled $K_a \rightarrow K_a'(p)$, where $p = 1$ and 2 denote the two components of the acceptor tunneling bundle (Figure 1). A large number of transitions are seen in the CRD spectrum in Figure 3. Due to the high resolution, broad and sharp spectral features are clearly distinguishable. The broad features have been assigned to water dimer, while the many sharp lines are associated with H_2O and the H_2O·Ar complex, both of which are present in the jet-expansion. The CRD spectra were also obtained with Ne and Kr as the carrier gas to further ensure that the broad features are from water dimer and not from H_2O·Ar.[14]

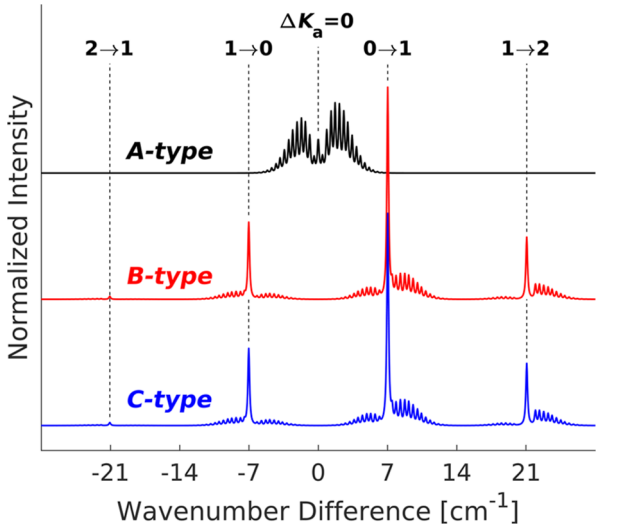

Figure 2. Generic rigid-rotor A-, B-, and C-type rotational profiles of water dimer.

https://doi.org/10.1021/acs.jpca.3c03705
J. Phys. Chem. A 2023, 127, 9409−9418

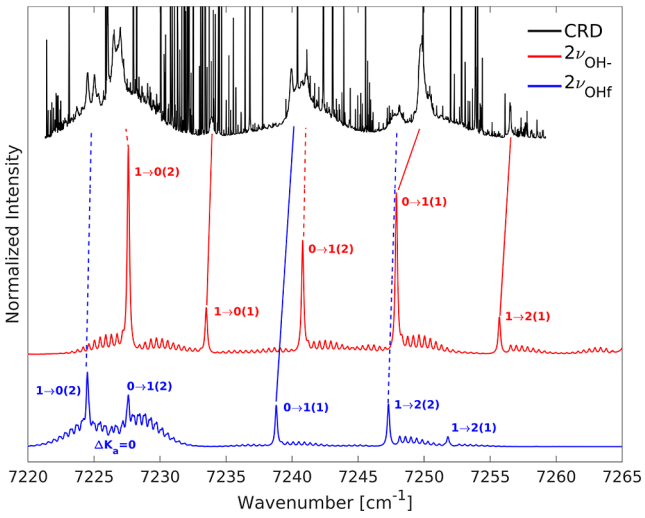

Figure 3. Calculated and experimental spectra in the 7220−7265 cm^{-1} range of the $\Delta\nu_{OH}$ = 2 region. The black trace is the jet-expansion CRD spectrum from ref 14, with Ar as the carrier gas and a rotational temperature of 10 ± 3 K. The red and blue traces show the spectral contribution from $2\nu_{OH\_}$ and $2\nu_{OH_f}$, respectively, simulated at T = 10 K. Both calculated vibrational bands (12D results in Table 2 for band origins) are shifted by +6.0 cm^{-1} to improve comparison with the experiment.

Our calculated band origins, including the empirical shift of +6 cm^{-1}, are 7227.2 (7221.2 + 6) cm^{-1} for $2\nu_{OH_f}$ and 7238.1 (7232.1 + 6) cm^{-1} for $2\nu_{OH\_}$. As seen in Figure 3, the sub-bands of each vibrational band are spread over a much larger wavenumber range than the calculated difference of 11 cm^{-1} between the two vibrational band origins. The pronounced overlap of the two vibrational bands makes the assignment of the individual observed sub-bands difficult without the aid of sophisticated models. As seen in the calculated spectrum in Figure 3, our model is capable of capturing each sub-band of the measured spectrum. The good agreement illustrates the accuracy of the calculated transition wavenumbers and relative intensities [VibMEMIC, CCSD(T)-F12/cc-pVTZ-F12 PES and DMF], as well as the importance of accounting for the acceptor tunneling splitting (GENIUSH, MB-pol PES).

As explained in ref 14, the nuclear spin statistical weights lead to $K_a \rightarrow K_a'(2)$ sub-bands with three Q branches (ΔJ = 0), whereas the $K_a \rightarrow K_a'(1)$ sub-bands have one Q branch. Our assignment of the observed sub-bands is consistent with this. This is seen in Figure 3, where, for example, the Q branch of the 1 → 0(2) sub-band of $2\nu_{OH\_}$ is clearly split in the experimental spectrum, whereas the 1 → 2(1) sub-band has a single Q branch.

We predict additional sub-bands for $2\nu_{OH\_}$ at slightly higher wavenumbers than the spectral region shown in Figure 3. First, a strong 1 → 2(2) sub-band is located at 7265.6 (7259.6 + 6) cm^{-1}, which is in excellent agreement with a strong sub-band observed in the experiment at ∼7267 cm^{-1}. This band shows clear Q branch splitting, in agreement with the proposed assignment. Second, a weak sub-band is observed at ∼7277.7 cm^{-1}, which also agrees with the predicted weak 2 → 3(2) sub-band at 7276.0 (7270.0 + 6) cm^{-1}.[14]

In addition to the two strongest and overlapping vibrational bands shown in Figure 3, we have simulated the spectra of the other three vibrational transitions that are predicted to have significant intensity in the $\Delta\nu_{OH}$ = 2 region (Table 2). In Figure 4, we present calculated spectra in the regions of the $2\nu_{OH_b}$, $2\nu_{OH\_}$, and $\nu_{OH_b} + \nu_{OH_f}$ bands. The predicted transition wavenumbers are 7051.9 (7045.9 + 6) cm^{-1} for $2\nu_{OH_b}$, 7193.6 (7187.6 + 6) cm^{-1} for $2\nu_{OH\_}$, and 7366.9 (7360.9 + 6) cm^{-1} for $\nu_{OH_b} + \nu_{OH_f}$.

As seen in the left panel of Figure 4, $2\nu_{OH_b}$ is almost exclusively an A-type band, and it is substantially red-shifted compared to the other OH-stretching transitions. Due to the large redshift, $2\nu_{OH_b}$ is located outside of the wavenumber range of the published experimental jet-expansion spectra.[10,14] This band has been observed in a Ne-matrix experiment at 7018 cm^{-1}, with a determined intensity of ∼0.4% relative to that of ν_{OH_b}.[12] In the Ne matrix, ν_{OH_b} was observed at 3590.5 cm^{-1},[12] which is approximately 10 cm^{-1} lower than the gas-phase (jet-cooled) value of 3601 cm^{-1}.[8] For $2\nu_{OH_b}$, the corresponding difference between the Ne matrix and the gas phase is expected to be larger. In a 1D picture, both the frequency and anharmonicity of the bound OH-stretch change and the transition wavenumber of $2\nu_{OH_b}$ cannot be predicted solely based on the observations of ν_{OH_b}. Our predicted transition wavenumber of 7051.9 (7045.9 + 6) cm^{-1} is about 30 cm^{-1} higher than that observed in the Ne matrix, and the predicted intensity is ∼0.2% relative to that of ν_{OH_b} (Tables 2 and S2).

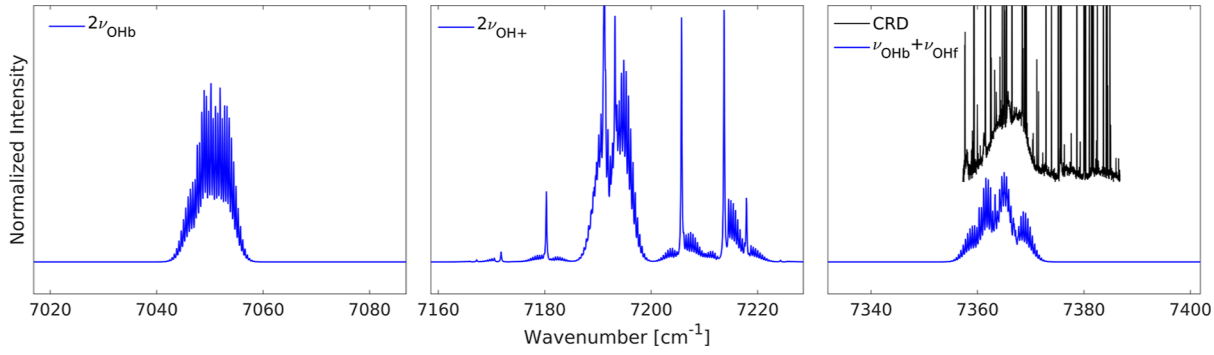

Figure 4. Spectra of the $2\nu_{OH_b}$, $2\nu_{OH\_}$, and $\nu_{OH_b} + \nu_{OH_f}$ bands. The black trace is a jet-expansion CRD spectrum from ref 14 (inset). The intensity and wavenumber ranges are the same in all three panels, and the relative areas in the different panels reflect the calculated relative oscillator strengths.

https://doi.org/10.1021/acs.jpca.3c03705
J. Phys. Chem. A 2023, 127, 9409−9418

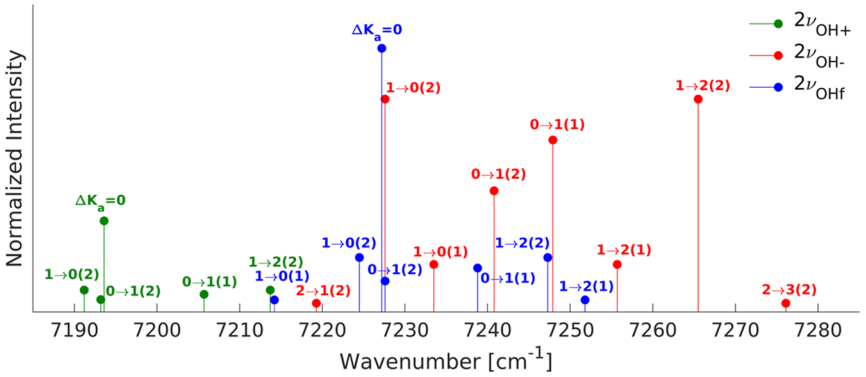

Figure 5. Calculated stick spectrum of the rotational−vibrational transitions of $2\nu_{OH_+}$ (green), $2\nu_{OH_f}$ (blue), and $2\nu_{OH_-}$ (red), with intensities corresponding to T = 10 K. The intensities of the ΔK_a = 0 sticks are the sum of intensities for the transitions with ΔK_a = 0, i.e., 0 → 0, 1 → 1, and 2 → 2. The calculated sticks are shifted by +6 cm^{-1} to improve comparison with experiments. The calculated vibrational transition wavenumbers are 7193.6 (7187.6 + 6) cm^{-1} for $2\nu_{OH_+}$, 7227.2 (7221.2 + 6) cm^{-1} for $2\nu_{OH_f}$, and 7238.1 (7232.1 + 6) cm^{-1} for $2\nu_{OH_-}$.

The predicted transition wavenumber of $2\nu_{OH_+}$ (Figure 4, middle panel) is within the reported spectral ranges of both jet-cooled experiments, and a band with an origin at ∼7192 cm^{-1} was observed in both jet-cooled experimental spectra.[10,14] Based on our 12D calculations, this band is unequivocally assigned to $2\nu_{OH_+}$. The calculated band of $2\nu_{OH_+}$ is A/C-type, with approximately equal contributions from both components based on the calculated direction of the transition dipole moment (Table S3). The A-type band structure is clearly observed in the experimental spectra, but the C-type band structure of this band has not been reported.

In the right panel of Figure 4, we compare the simulated spectrum of the most intense combination band, $\nu_{OH_b} + \nu_{OH_f}$, with the experimental CRD spectrum.[14] A broad band with a maximum at ∼7366 cm^{-1} is observed in the CRD spectrum. This band was previously assigned to an unknown larger water multimer. The calculated transition wavenumber and the A-type band profile of $\nu_{OH_b} + \nu_{OH_f}$ agree well with the observed band. No other strong water dimer transitions are predicted in the 7357−7386 cm^{-1} region, and we assign the observed band centered around ∼7366 cm^{-1} as $\nu_{OH_b} + \nu_{OH_f}$.

In Figure 5, we present an overview of the calculated $K_a \rightarrow K_a'(p)$ transitions in the 7190−7280 cm^{-1} spectral region. In ref 14, the sub-bands in this region were tentatively assigned to four vibrational bands, $\nu_{OH_b} + \nu_{OH_f}$, $2\nu_{OH_+}$, $2\nu_{OH_f}$, and $2\nu_{OH_-}$, with origins at 7192.34, 7225.86, 7240.57, and 7256.99 cm^{-1}, respectively. We reassign the experimentally observed sub-bands in this region to only three vibrational transitions: $2\nu_{OH_+}$, $2\nu_{OH_f}$, and $2\nu_{OH_-}$. The determined vibrational band origins depend on the assignment of the sub-bands. We assign the band origins of $2\nu_{OH_f}$ and $2\nu_{OH_-}$ to ∼7227 and ∼7238 cm^{-1}, respectively, based on our calculated vibrational transition wavenumbers (Table 2, +6 cm^{-1} shift). The previously determined experimental band origin at 7192.34 cm^{-1} is assigned to the $2\nu_{OH_+}$ band. In addition, we assign the band at ∼7366 cm^{-1} to $\nu_{OH_b} + \nu_{OH_f}$.[14]

CONCLUSIONS

We have extended the VibMEMIC model to include transition intensities and used it to calculate intramolecular transitions in water dimer. We have calculated vibrational transition wavenumbers and intensities in the fundamental HOH-bending, fundamental OH-stretching, first OH-stretching-HOH-bending combination, and first OH-stretching overtone regions. The rotational−vibrational spectrum of water dimer was calculated in the first OH-stretching overtone region at a temperature of 10 K, corresponding to the temperature of the existing jet-expansion experiments.[10,14] The calculated spectrum was obtained by combining vibrational band origins and transition intensities calculated with a full-dimensional (12D) vibrational model [VibMEMIC, CCSD(T)-F12/cc-pVTZ-F12 PES and DMF] with vibrational−rotational-tunneling energy levels calculated with reduced-dimensional models performed with the GENIUSH code (MB-pol PES). The spectrum in the first OH-stretching overtone region, 7000−7500 cm^{-1}, is complicated by multiple vibrational−rotational-tunneling sub-bands. With our calculated spectrum, we were able to assign all observed vibrational−rotational-tunneling sub-bands in the first OH-stretching overtone region. Based on the new assignment, the vibrational band origins are 7192.34, ∼7227, ∼7238, and ∼7366 cm^{-1} for $2\nu_{OH_+}$, $2\nu_{OH_f}$, $2\nu_{OH_-}$, and $\nu_{OH_b} + \nu_{OH_f}$, respectively.

Experimental vibrational transition wavenumbers are important for benchmarking calculations, e.g., to improve model development. For hydrogen-bonded complexes, the literature on accurate intramolecular transition wavenumbers is sparse. The experimental spectra in refs 10 and 14 contain valuable information that helps advance our understanding of infrared absorption spectra of hydrogen-bonded complexes, with the water dimer being the archetype of such complexes. However, as illustrated here, accurate rotational−vibrational models are needed to guide the assignment of complicated spectra associated with these complexes and, subsequently, to determine experimental vibrational band origins.

ASSOCIATED CONTENT

Supporting Information

The Supporting Information is available free of charge at https://pubs.acs.org/doi/10.1021/acs.jpca.3c03705.

Coordinate definition; further details of the VibMEMIC calculations; calculated transition wavenumbers, intensities, and transition dipole moments with 6D and 12D models; list of all transitions in different intramolecular regions, further details of the GENIUSH calculations;

https://doi.org/10.1021/acs.jpca.3c03705
J. Phys. Chem. A 2023, 127, 9409−9418

state-specific rotation-tunneling energy-level patterns; symmetry considerations for reduced-dimensional calculations; and computed VRT transitions (PDF)

AUTHOR INFORMATION

Corresponding Author

Henrik G. Kjaergaard − *Department of Chemistry, University of Copenhagen, Copenhagen Ø DK-2100, Denmark;* orcid.org/0000-0002-7275-8297; Email: hgk@chem.ku.dk

Authors

Emil Vogt − *Department of Chemistry, University of Copenhagen, Copenhagen Ø DK-2100, Denmark;* orcid.org/0000-0003-3335-9813

Irén Simkó − *Laboratory of Molecular Structure and Dynamics, Institute of Chemistry ELTE Eötvös Loránd University, Budapest H-1117, Hungary; HUN-REN−ELTE Complex Chemical Systems Research Group, Budapest 112 H-1518, Hungary;* Present Address: New York University, Simons Center for Computational Physical Chemistry, 24 Waverly Place, New York, New York 10003, United States

Attila G. Császár − *Laboratory of Molecular Structure and Dynamics, Institute of Chemistry ELTE Eötvös Loránd University, Budapest H-1117, Hungary; HUN-REN−ELTE Complex Chemical Systems Research Group, Budapest 112 H-1518, Hungary;* orcid.org/0000-0001-5640-191X

Complete contact information is available at: https://pubs.acs.org/10.1021/acs.jpca.3c03705

Notes

The authors declare no competing financial interest.

ACKNOWLEDGMENTS

We thank Robert Georges, Michel Herman, David J. Nesbitt, and Sergey A. Nizkorodov for sharing their experimental data. We are grateful for funding from the Independent Research Fund Denmark (grant no. 9040-00142B), the Novo Nordisk Foundation (grant no. NNF220C0080193), and the National Research, Development, and Innovation Fund of Hungary (NKFIH, grant no. K138233), and for computer time from the High-Performance Center at the Faculty of Science at the University of Copenhagen.

REFERENCES

(1) Scheiner, S. Ab initio studies of hydrogen bonds: the water dimer paradigm. *Annu. Rev. Phys. Chem.* **1994**, *45*, 23−56.

(2) Mukhopadhyay, A.; Cole, W. T.; Saykally, R. J. The water dimer I: Experimental characterization. *Chem. Phys. Lett.* **2015**, *633*, 13−26.

(3) Mukhopadhyay, A.; Xantheas, S. S.; Saykally, R. J. The water dimer II: Theoretical investigations. *Chem. Phys. Lett.* **2018**, *700*, 163−175.

(4) Vogt, E.; Kjaergaard, H. G. Vibrational spectroscopy of the water dimer at jet-cooled and atmospheric temperatures. *Annu. Rev. Phys. Chem.* **2022**, *73*, 209−231.

(5) Van Thiel, M.; Becker, E. D.; Pimentel, G. C. Infrared studies of hydrogen bonding of water by the matrix isolation technique. *J. Chem. Phys.* **1957**, *27*, 486−490.

(6) Page, R. H.; Frey, J. G.; Shen, Y.-R.; Lee, Y. Infrared predissociation spectra of water dimer in a supersonic molecular beam. *Chem. Phys. Lett.* **1984**, *106*, 373−376.

(7) Huang, Z. S.; Miller, R. E. High-resolution near-infrared spectroscopy of water dimer. *J. Chem. Phys.* **1989**, *91*, 6613−6631.

(8) Huisken, F.; Kaloudis, M.; Kulcke, A. Infrared spectroscopy of small size-selected water clusters. *J. Chem. Phys.* **1996**, *104*, 17−25.

(9) Paul, J. B.; Provencal, R. A.; Chapo, C.; Roth, K.; Casaes, R.; Saykally, R. J. Infrared cavity ringdown spectroscopy of the water cluster bending vibrations. *J. Phys. Chem. A* **1999**, *103*, 2972−2974.

(10) Nizkorodov, S. A.; Ziemkiewicz, M.; Nesbitt, D. J.; Knight, A. E. W. Overtone spectroscopy of H_2O clusters in the ν_{OH}=2 manifold: Infrared-ultraviolet vibrationally mediated dissociation studies. *J. Chem. Phys.* **2005**, *122*, 194316.

(11) Kuyanov-Prozument, K.; Choi, M. Y.; Vilesov, A. F. Spectrum and infrared intensities of OH-stretching bands of water dimers. *J. Chem. Phys.* **2010**, *132*, 014304.

(12) Bouteiller, Y.; Tremblay, B.; Perchard, J. P. The vibrational spectrum of the water dimer: Comparison between anharmonic ab initio calculations and neon matrix infrared data between 14,000 and 90 cm^{-1}. *Chem. Phys.* **2011**, *386*, 29−40.

(13) León, I.; Montero, R.; Castaño, F.; Longarte, A.; Fernández, J. A. Mass-resolved infrared spectroscopy of complexes without chromophore by nonresonant femtosecond ionization detection. *J. Phys. Chem. A* **2012**, *116*, 6798−6803.

(14) Suas-David, N.; Vanfleteren, T.; Földes, T.; Kassi, S.; Georges, R.; Herman, M. The water dimer investigated in the 2OH spectral range using cavity ring-down spectroscopy. *J. Phys. Chem. A* **2015**, *119*, 10022−10034.

(15) Schwan, R.; Qu, C.; Mani, D.; Pal, N.; van der Meer, L.; Redlich, B.; Leforestier, C.; Bowman, J. M.; Schwaab, G.; Havenith, M. Observation of the low-frequency spectrum of the water dimer as a sensitive test of the water dimer potential and dipole moment surfaces. *Angew. Chem., Int. Ed.* **2019**, *58*, 13119−13126.

(16) León, I.; Montero, R.; Longarte, A.; Fernández, J. A. Revisiting the spectroscopy of water dimer in jets. *J. Phys. Chem. Lett.* **2021**, *12*, 1316−1320.

(17) Zhang, B.; Yu, Y.; Zhang, Z.; Zhang, Y.-Y.; Jiang, S.; Li, Q.; Yang, S.; Hu, H.-S.; Zhang, W.; Dai, D.; et al. Infrared spectroscopy of neutral water dimer based on a tunable vacuum ultraviolet free electron laser. *J. Phys. Chem. Lett.* **2020**, *11*, 851−855.

(18) Coker, D. F.; Miller, R. E.; Watts, R. O. The infrared predissociation spectra of water clusters. *J. Chem. Phys.* **1985**, *82*, 3554−3562.

(19) Buck, U.; Huisken, F. Infrared spectroscopy of size-selected water and methanol clusters. *Chem. Rev.* **2000**, *100*, 3863−3890.

(20) Schofield, D. P.; Kjaergaard, H. G. Calculated OH-stretching and HOH-bending vibrational transitions in the water dimer. *Phys. Chem. Chem. Phys.* **2003**, *5*, 3100−3105.

(21) Kjaergaard, H. G.; Garden, A. L.; Chaban, G. M.; Gerber, R. B.; Matthews, D. A.; Stanton, J. F. Calculation of vibrational transition frequencies and intensities in water dimer: Comparison of different vibrational approaches. *J. Phys. Chem. A* **2008**, *112*, 4324−4335.

(22) Mackeprang, K.; Kjaergaard, H. G.; Salmi, T.; Hänninen, V.; Halonen, L. The effect of large amplitude motions on the transition frequency redshift in hydrogen bonded complexes: A physical picture. *J. Chem. Phys.* **2014**, *140*, 184309.

(23) Mackeprang, K.; Hänninen, V.; Halonen, L.; Kjaergaard, H. G. The effect of large amplitude motions on the vibrational intensities in hydrogen bonded complexes. *J. Chem. Phys.* **2015**, *142*, 094304.

(24) Dyke, T. R. Group theoretical classification of the tunneling−rotational energy levels of water dimer. *J. Chem. Phys.* **1977**, *66*, 492−497.

(25) Bunker, P. R.; Jensen, P. *Molecular Symmetry and Spectroscopy*; NRC Research Press: Ottawa, 2006; pp 28−51.

(26) Huang, X.; Braams, B. J.; Bowman, J. M.; Kelly, R. E. A.; Tennyson, J.; Groenenboom, G. C.; van der Avoird, A. New ab initio potential energy surface and the vibration-rotation-tunneling levels of $(H_2O)_2$ and $(D_2O)_2$. *J. Chem. Phys.* **2008**, *128*, 034312.

(27) Shank, A.; Wang, Y.; Kaledin, A.; Braams, B. J.; Bowman, J. M. Accurate ab initio and "hybrid" potential energy surfaces, intramolecular vibrational energies, and classical IR spectrum of the water dimer. *J. Chem. Phys.* **2009**, *130*, 144314.

(28) Wang, Y.; Huang, X.; Shepler, B. C.; Braams, B. J.; Bowman, J. M. Flexible, ab initio potential, and dipole moment surfaces for water. I. Tests and applications for clusters up to the 22-mer. *J. Chem. Phys.* **2011**, *134*, 094509.
(29) Babin, V.; Leforestier, C.; Paesani, F. Development of a "first principles" water potential with flexible monomers: Dimer potential energy surface, VRT Spectrum, and second virial coefficient. *J. Chem. Theory Comput.* **2013**, *9*, 5395−5403.
(30) Leforestier, C.; Szalewicz, K.; van der Avoird, A. Spectra of water dimer from a new *ab initio* potential with flexible monomers. *J. Chem. Phys.* **2012**, *137*, 014305.
(31) Jankowski, P.; Murdachaew, G.; Bukowski, R.; Akin-Ojo, O.; Leforestier, C.; Szalewicz, K. Ab initio water pair potential with flexible monomers. *J. Phys. Chem. A* **2015**, *119*, 2940−2964.
(32) Metz, M. P.; Szalewicz, K. Automatic generation of flexible-monomer intermolecular potential energy surfaces. *J. Chem. Theory Comput.* **2020**, *16*, 2317−2339.
(33) Yu, Q.; Qu, C.; Houston, P. L.; Conte, R.; Nandi, A.; Bowman, J. M. q-AQUA: A many-body CCSD(T) water potential, including four-body interactions, demonstrates the quantum nature of water from clusters to the liquid phase. *J. Phys. Chem. Lett.* **2022**, *13*, 5068−5074.
(34) Rocher-Casterline, B. E.; Ch'ng, L. C.; Mollner, A. K.; Reisler, H. Communication: Determination of the bond dissociation energy (D_0) of the water dimer, $(H_2O)_2$, by velocity map imaging. *J. Chem. Phys.* **2011**, *134*, 211101.
(35) Lane, J. R. CCSDTQ optimized geometry of water dimer. *J. Chem. Theory Comput.* **2013**, *9*, 316−323.
(36) Lee, V. G. M.; McCoy, A. B. An efficient approach for studies of water clusters using diffusion Monte Carlo. *J. Phys. Chem. A* **2019**, *123*, 8063−8070.
(37) Leforestier, C.; Gatti, F.; Fellers, R. S.; Saykally, R. J. Determination of a flexible (12D) water dimer potential via direct inversion of spectroscopic data. *J. Chem. Phys.* **2002**, *117*, 8710−8722.
(38) Scribano, Y.; Leforestier, C. Contribution of water dimer absorption to the millimeter and far infrared atmospheric water continuum. *J. Chem. Phys.* **2007**, *126*, 234301.
(39) Leforestier, C. Infrared shifts of the water dimer from the fully flexible ab initio HBB2 potential. *Philos. Trans. R. Soc., A* **2012**, *370*, 2675−2690.
(40) Wang, X.-G.; Carrington, T. Using monomer vibrational wavefunctions to compute numerically exact (12D) rovibrational levels of water dimer. *J. Chem. Phys.* **2018**, *148*, 074108.
(41) Wang, X.-G.; Carrington, T. Computing excited OH stretch states of water dimer in 12D using contracted intermolecular and intramolecular basis functions. *J. Chem. Phys.* **2023**, *158*, 084107.
(42) Vogt, E.; Simkó, I.; Császár, A. G.; Kjaergaard, H. G. Reduced-dimensional vibrational models of the water dimer. *J. Chem. Phys.* **2022**, *156*, 164304.
(43) Czakó, G.; Mátyus, E.; Császár, A. G. Bridging theory with experiment: a benchmark study of thermally averaged structural and effective spectroscopic parameters of the water molecule. *J. Phys. Chem. A* **2009**, *113*, 11665−11678.
(44) Fábri, C.; Mátyus, E.; Császár, A. G. Rotating full- and reduced-dimensional quantum chemical models of molecules. *J. Chem. Phys.* **2011**, *134*, 074105.
(45) Fábri, C.; Quack, M.; Császár, A. G. On the use of nonrigid-molecular symmetry in nuclear-motion computations employing a discrete variable representation: a case study of the bending energy levels of CH_5^+. *J. Chem. Phys.* **2017**, *147*, 134101.
(46) Kjaersgaard, A.; Vogt, E.; Hansen, A. S.; Kjaergaard, H. G. Room temperature gas-phase detection and Gibbs energies of water amine bimolecular complex formation. *J. Phys. Chem. A* **2020**, *124*, 7113−7122.
(47) Vogt, E.; Bertran Valls, P.; Kjaergaard, H. G. Accurate calculations of OH-Stretching intensities with a reduced-dimensional local mode model including Eckart axis embedding. *J. Phys. Chem. A* **2020**, *124*, 932−942.
(48) Hansen, A. S.; Huchmala, R. M.; Vogt, E.; Boyer, M. A.; Bhagde, T.; Vansco, M. F.; Jensen, C. V.; Kjærsgaard, A.; Kjaergaard, H. G.; McCoy, A. B.; Lester, M. I. Coupling of torsion and OH-stretching in tert-butyl hydroperoxide. I. The cold and warm first OH-stretching overtone spectrum. *J. Chem. Phys.* **2021**, *154*, 164306.
(49) Vogt, E.; Huchmala, R. M.; Jensen, C. V.; Boyer, M. A.; Wallberg, J.; Hansen, A. S.; Kjærsgaard, A.; Lester, M. I.; McCoy, A. B.; Kjaergaard, H. G. Coupling of torsion and OH-stretching in tert-butyl hydroperoxide. II. The OH-stretching fundamental and overtone spectra. *J. Chem. Phys.* **2021**, *154*, 164307.
(50) Carter, S.; Culik, S. J.; Bowman, J. M. Vibrational self-consistent field method for many-mode systems: a new approach and application to the vibrations of CO adsorbed on Cu (100). *J. Chem. Phys.* **1997**, *107*, 10458−10469.
(51) Bowman, J. M.; Carrington, T.; Meyer, H.-D. Variational quantum approaches for computing vibrational energies of polyatomic molecules. *Mol. Phys.* **2008**, *106*, 2145−2182.
(52) Western, C. M. PGOPHER: A program for simulating rotational, vibrational and electronic spectra. *J. Quant. Spectrosc. Radiat. Transfer* **2017**, *186*, 221−242.
(53) Wang, Y.; Carter, S.; Braams, B. J.; Bowman, J. M. MULTIMODE quantum calculations of intramolecular vibrational energies of the water dimer and trimer using ab initio-based potential energy surfaces. *J. Chem. Phys.* **2008**, *128*, 071101.
(54) Arunan, E.; Desiraju, G. R.; Klein, R. A.; Sadlej, J.; Scheiner, S.; Alkorta, I.; Clary, D. C.; Crabtree, R. H.; Dannenberg, J. J.; Hobza, P.; et al. Definition of the hydrogen bond (IUPAC Recommendations 2011). *Pure Appl. Chem.* **2011**, *83*, 1637−1641.
(55) Salmi, T.; Hänninen, V.; Garden, A. L.; Kjaergaard, H. G.; Tennyson, J.; Halonen, L. Calculation of the O-H stretching vibrational overtone spectrum of the water dimer. *J. Phys. Chem. A* **2008**, *112*, 6305−6312.
(56) Otto, K. E.; Xue, Z.; Zielke, P.; Suhm, M. A. The Raman spectrum of isolated water clusters. *Phys. Chem. Chem. Phys.* **2014**, *16*, 9849−9858.

https://doi.org/10.1021/acs.jpca.3c03705
J. Phys. Chem. A 2023, 127, 9409−9418